LOW EMITTANCE BEAM TRANSPORT SYSTEM OF THE POSITION DAMPING RING FOR THE SUPER TAU CHARM FACILITY*

Xu Yang[1], Ruixuan Huang†,[1], Binghao Zhang[1], Zhouyu Zhao[1], Jingyu Tang[1], Youjin Yuan[2]
[1]University of Science and Technology of China, Hefei, China
[2]Institute of Modern Physics, Chinese Academy of Sciences, Lanzhou, China

Abstract

The Super Tau-Charm Facility is a high-luminosity electron–positron collider operating at a center-of-mass energy range of 2–7 GeV. The stringent requirements for beam brightness and stability pose significant challenges to the injector transport system, especially the positron transport lines of the damping ring. Beam transverse emittance is one of the primary parameters, which is influenced by a mass of components in the lattice design. In this study, a newly developed multistage optimization method is employed to optimize multiple sets of quadrupole strengths along the transport line. The optimized results effectively suppress the emittance growth and maintain compliance of other parameters with damping ring requirements. These results provide a practical reference for the optical design of high-brightness transport systems in next-generation electron–positron colliders.

INTRODUCTION

The Super Tau-Charm Facility (STCF), a next-generation high-luminosity electron–positron collider, is designed to achieve a peak luminosity of 5×10^{34} cm^{-2} s^{-1} at a center-of-mass energy range of 2-7 GeV [1]. This requires high beam brightness, stability, and injection efficiency, making beam quality preservation in the injector transport system critical for overall performance. The main components of beam transport system includes three parts: injection line from the position linac to the damping ring, extraction line from damping ring to main linac, and injection lines from main linac to the collider rings. A preliminary lattice design for the STCF beam transport system has been developed, where the optics matching and emittance preservation was realized [2]. However, the previous beam dynamics optimization was based on an ideal Gaussian beam model. With a more realistic beam distribution, simulations reveal substantial emittance growth and dispersion distortion, indicating limited robustness of the current optimization method. The inclusion of coherent/incoherent synchrotron radiation effects further complicates the beam dynamics and imposes more stringent requirements on lattice optimization [3]. This issue is of greater concern for the positron beam. In this work, we focus on further optimization of the positron beam, thereby enabling the design of a low-emittance transport line under a non-ideal beam model.

* Work supported by the National Key R&D Program of China under Contract No. 2022YFA1602202, the National Natural Science Foundation of China (No.12341501 and 12175224) and the STCF key technology research and development project.
† rxhuang@ustc.edu.cn

In the injection transport line of the STCF damping ring, it consists of a horizontal bending arc with eight 15° dipoles, a chicane-based energy-spread compression system with four 30° dipoles and one 1.6 m accelerating structure, and a matching section with one 10° dipole. Standard FODO cells (40 quadrupoles in total) are used for beam focusing and optics matching (Fig. 1).

Under a fixed lattice configuration, where component positions are fixed, optimizing quadrupole strengths to suppress emittance growth and enhance beam transport remains extremely challenging. The strongly coupled parameters and reliance on numerical simulations make this a high-dimensional black-box problem, limiting the effectiveness of gradient-based methods and making exhaustive parameter scans computationally expensive.

MULTISTAGE BO-NSGAII OPTIMIZATION METHOD

In this study, the strengths of the 31 quadrupole magnets along the beamline are treated as optimization variables. The corresponding optimization problem is formulated in Eq. (1).

$$\begin{aligned} x^* &= \arg\min_{x\in X} f_i(x), \quad i\in\{1,\ldots,n\} \\ \text{s.t.} \quad & c_j(x)\le 0, \quad j\in\{1,\ldots,m\} \end{aligned} \tag{1}$$

Here, $f_i(x)$ denotes the optimization objectives, $c_j(x)$ represents the constraint conditions, and all variables x are confined within the specified range X.

The objectives considered in this work include the dispersion functions (η_x, η_x'), Twiss parameters (β_x, β_y, α_x, α_y) at the beamline exit, and the transverse emittances (ε_x, ε_y). Constraints are imposed on the global maximum β-function along the transport line to limit beam size growth. β and η are given in meters, while the emittances ε are given in nm·rad. To lower the complexity of the optimization, objectives of the same category are combined, as shown in Eq. (2). The initial transverse emittances at the starting point are $\varepsilon_{x0} = 466.31$ nm·rad and $\varepsilon_{y0} = 663.12$ nm·rad. The final target values for the beta functions at the exit were set to $\beta_{x\_target} = 9.61$ m and $\beta_{y\_target} = 3.98$ m.

$$\begin{aligned} f_1 &= \Delta\varepsilon = \frac{\varepsilon_x-\varepsilon_{x0}}{\varepsilon_{x0}} + \frac{\varepsilon_y-\varepsilon_{y0}}{\varepsilon_{y0}} \\ f_2 &= |\eta_x| + |\eta_x'| \\ f_3 &= \Delta\beta = |\beta_x-\beta_{x\_target}| + |\beta_y-\beta_{y\_target}| \\ f_4 &= \alpha = |\alpha_x| + |\alpha_y| \\ c &= \max(\beta) < 100 \end{aligned} \tag{2}$$

A multistage optimization framework integrating Bayesian Optimization (BO) [4-6] and the Non-dominated Sorting Genetic Algorithm II (NSGA-II) [7-8] is developed to optimize a non-ideal beam in a fixed lattice. Starting from

a preliminary transport line design, the procedure proceeds in three sequential stages (Fig. 1).

In the first two stages, BO regulates both the transverse emittance variation Δε and the dispersion-related metric $|\eta_x| + |\eta_x'|$, optimizing strengths of 9 quadrupoles in the first stage (the horizontal bending are arranged symmetrically) and 12 in the second. In the final stage, NSGA-II simultaneously addresses all optimization objectives, adjusting the remaining 10 quadrupole strengths. In addition, several high-performing solutions from the preceding stage were selected, and their variables were fixed, based on which the current stage of optimization was carried out.

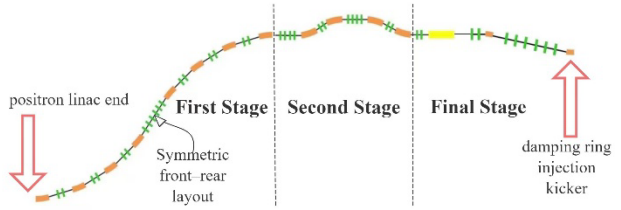

Figure 1: Transport line lattice design: Black is the drift section; Orange is the bending magnet; Green is the quadrupole magnet; Yellow is the accelerating cavity.

Combining the theoretical foundations of BO and NSGA-II with an Elegant-based [9] automation workflow for parameter adjustment and data retrieval, we establish a robust multistage optimization strategy (Fig. 2).

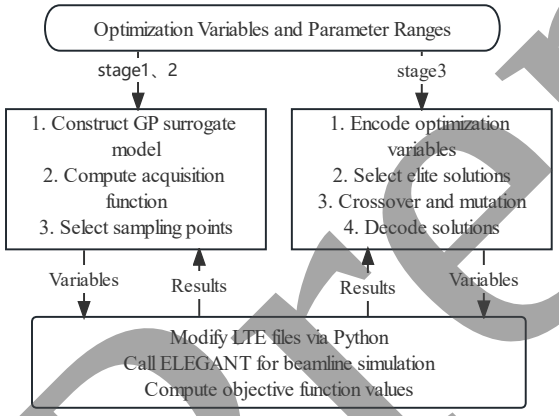

Figure 2: Flowchart of the multistage optimization process.

OPTIMIZATION RESUTLS

The initial two stages of accelerator lattice optimization employed BO and NSGA-II. The BO process utilized 200 random initial samples and 600 iterations (simulating 800 evaluations), while NSGA-II was configured with a population of 200 evolved over 50 generations (simulating to 10,000 evaluations). The results demonstrate that BO significantly outperforms NSGA-II in sampling efficiency and solution quality for a limited number of objectives (Fig. 3). During this process, the dispersion function was maintained at zero, and Δε was constrained within 14 % and 12 %, establishing a robust foundation for the final-stage optimization.

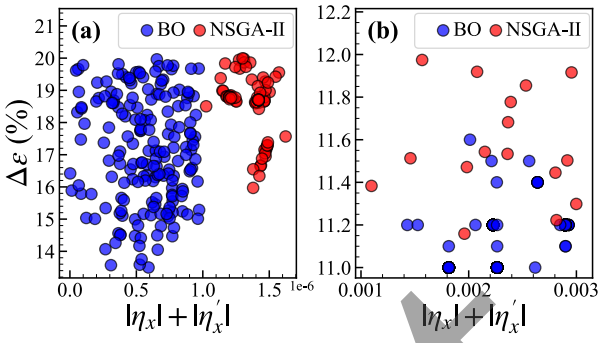

Figure 3: Optimization results of stage 1 (a) and stage 2 (b) using BO and NSGA-II.

In the final stage, a multi-objective optimization was performed using the NSGA-II algorithm, with an initial population of 600 and 100 generations. This approach effectively maintained Δε below 15 % and $|\eta_x| + |\eta_x'|$ below 0.001 while ensuring satisfactory Twiss parameter matching (Fig. 4).

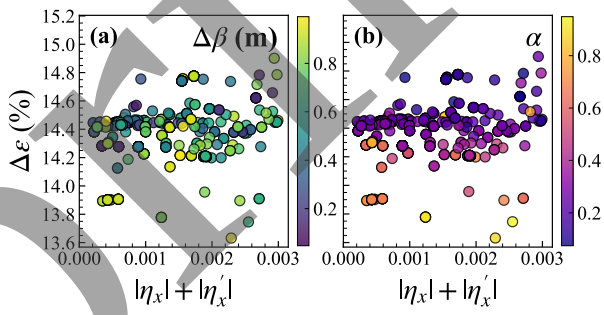

Figure 4: Final-stage optimization results.

The optimization performance was evaluated using the normalized distance d to the minimum of each objective, as defined in Eq. 3. Minimum points were determined from the complete dataset to enable consistent normalization, with f_{1_min}, f_{2_min}, f_{3_min} and f_{4_min} set to 5.0017 %, 8.8×10^{-5}, 0.0234 m and 0.0017.

$$d = \sqrt{\sum_{i=1}^{i=4} \left(\frac{f_i - f_{i\_min}}{f_{i\_min}}\right)^2} \quad (3)$$

Three optimization strategies were evaluated. First, all 31 variables were directly optimized using NSGA-II. Second, the first 21 variables were fixed using either BO or NSGA-II, followed by final-stage optimization of the remaining 10 variables (Fig. 5).

The multistage optimization solutions exhibit dispersion functions on the order of 10^{-3} and Twiss parameter deviations within 0.1, whereas globally optimized solutions show poorer performance with dispersion functions around 10^{-2} and Twiss deviations exceeding 1. Furthermore, when the first 21 variables are fixed using BO, convergence is achieved within 13,000 simulations in the final stage. In contrast, fixing the same 21 variables with NSGA-II requires 23,000 simulations for convergence, with slightly inferior solution quality.

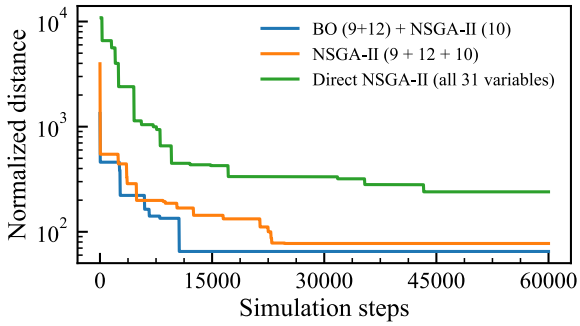

Figure 5: Staged and global optimization convergence

A representative data was selected from the final results to illustrate the optimization. The final dispersion function was maintained at zero, and the Twiss parameters satisfied design requirements, while emittance growth was effectively controlled (Fig. 6) .

Table 1 summarizes the beamline exit parameters for the unoptimized design—representing a preliminary design with a non-ideal beam—and the optimized design. With initial emittances εx0 = 466.31 nm·rad and εy0 = 663.12 nm·rad, the unoptimized design yielded exit values of 483.68 and 1065.17 nm·rad, whereas the optimized design reduced them to 479.31 and 742.65 nm·rad. The current optimization success-fully decreased Δε from 64.36 % to 14.78 %, reduced Δβ from 5.02 m to 0.1 m, and adjusted α from 0.5658 to 0.0752.

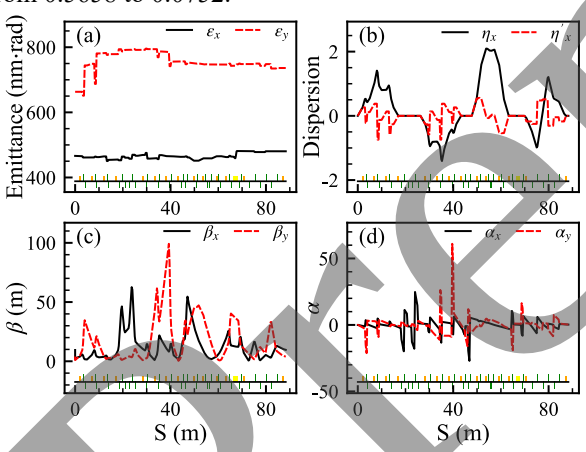

Figure 6: Evolution of emittance (a), dispersion functions (b), and Twiss parameters (c, d); The lower panel is the transport line lattice layout.

Table 1: Beamline Exit Parameters

Parameters	Unoptimized	Optimized
$\varepsilon_{x/y}$ [nm•rad]	483.68/1065.17	479.31/742.65
η_x [m]	-1.203×10^{-3}	9.013×10^{-4}
η_x'	-2.891×10^{-4}	-1.812×10^{-4}
$\beta_{x/y}$ [m]	8.03/0.54	9.64/4.05
$\alpha_{x/y}$	-0.3243/0.2415	-0.0168/0.0584
max_β [m]	149.41	99.18

The transverse phase space of the optimized design exhibits a more uniform and circular distribution compared to the unoptimized design, with reduced filamentation and denser core concentration (Fig. 7). This enhanced uniformity minimizes emittance growth and beam mismatch, ensuring compatibility with the acceptance and design requirements of the subsequent damping ring.

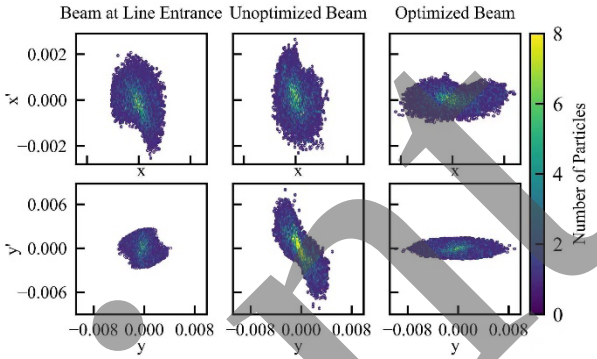

Figure 7: Transverse phase space at the entrance (left) and exit for the unoptimized (middle) and the optimized (right) design.

CONCLUSION

A multistage optimization framework combining BO and NSGA-II has been developed for the STCF positron damping ring injection transport line. 31 quadrupole strengths were treated as optimization variables to minimize transverse emittance, control the dispersion function, and adjust Twiss parameters at the beamline exit. After fixing the solutions obtained from the first two BO stages, the final stage achieved maximal convergence speed and solution quality. The optimized scheme reduces the emittance growth rate from 64.36% to 14.78%, exhibits a more uniform transverse phase space, and minimizes beam mismatch, fulfilling the design requirements for the downstream damping ring. These results demonstrate that the proposed multistage optimization method provides an efficient and effective solution for high-brightness beam transport in next-generation electron–positron colliders.

REFERENCES

[1] X. C. Ai, L. P. An, S. Z. An et al., "Conceptual design report of the Super Tau-Charm Facility: the accelerator," Nucl. Sci. Tech., vol. 36, p. 242, 2025. doi:10.1007/s41365-025-01833-x

[2] R. Huang, J. Tang, Z. Yu, et al., "Preliminary design of the beam transport system for the Super Tau-Charm Facility," preprint / conference report, 2025.

[3] S. Di Mitri, "Coherent synchrotron radiation and microbunching instability," CERN Yellow Rep., 2018. doi:10.23730/CYRSP-2018-001.381

[4] J. Mockus, "The Bayesian approach to global optimization," in Bayesian Approach to Global Optimization, Springer, Dordrecht, pp. 125–156, 1989.

[5] B. Shahriari, K. Swersky, Z. Wang, R. P. Adams, and N. de Freitas, "Taking the human out of the loop: A review of Bayesian optimization," Proc. IEEE, vol. 104, no. 1, pp. 148–175, 2016. doi:10.1109/JPROC.2015.2494218

[6] R. Roussel et al., "Bayesian optimization algorithms for accelerator physics," Phys. Rev. Accel. Beams, vol. 27, p. 084801, 2024. 127-136, 2024. doi:10.1103/PhysRevAccelBeams.27.084801

[7] K. Deb, A. Pratap, S. Agarwal, et al., "A fast and elitist multiobjective genetic algorithm: NSGA-II," IEEE Trans. Evol. Comput., vol. 6, no. 2, pp. 182–197, 2002. doi:10.1109/4235.996017

[8] M. Yarmohammadi Satri, A. M. Lombardi, and F. Zimmermann, "Multiobjective genetic algorithm approach to optimize beam matching and beam transport in high-intensity hadron linacs," Phys. Rev. Accel. Beams, vol. 22, p. 054201, 2019. doi:10.1103/PhysRevAccelBeams.22.054201

[9] M. Borland, "Elegant: A flexible SDDS-compliant code for accelerator simulation," Adv. Photon Source, LS-287, Sep. 2000. doi:10.2172/761286